Article

Doping Effects on Magnetic and Electronic Transport Properties in $BaZn_2As_2$

Guoqiang Zhao [1,2,3,†] (ID), Gangxu Gu [2,†], Shuai Yang [2,†], Yi Peng [2], Xiang Li [1], Kenji M. Kojima [4], Chaojing Lin [2], Xiancheng Wang [2,5], Timothy Ziman [1], Yasutomo J. Uemura [3] (ID), Bo Gu [1,5,*] (ID), Gang Su [1,6] (ID), Sadamichi Maekawa [1,7,8], Yongqing Li [2,5,*] and Changqing Jin [2,5,*]

1   Kavli Institute for Theoretical Sciences (KITS), University of Chinese Academy of Sciences, Beijing 101408, China; g.q.zhao@iphy.ac.cn (G.Z.)
2   Beijing National Laboratory for Condensed Matter Physics, Institute of Physics, Chinese Academy of Sciences, Beijing 100190, China
3   Department of Physics, Columbia University, New York, NY 10027, USA; yu2@columbia.edu
4   TRIUMF, Vancouver, BC V6T 2A3, Canada
5   School of Physics, University of Chinese Academy of Sciences, Beijing 101408, China
6   Institute of Theoretical Physics, Chinese Academy of Sciences, Beijing 100190, China
7   RIKEN Center for Emergent Matter Science (CEMS), Wako 315-0198, Japan
8   Advanced Science Research Center (ASRC), Japan Atomic Energy Agency, Tokai 319-1195, Japan
*   Correspondence: gubo@ucas.ac.cn (B.G.); yqli@iphy.ac.cn (Y.L.); jin@iphy.ac.cn (C.J.)
†   These authors contributed equally to this work.

Abstract: Novel diluted magnetic semiconductors derived from $BaZn_2As_2$ are of considerable importance owing to their elevated Curie temperature of 260 K, the diversity of magnetic states they exhibit, and their prospective applications in multilayer heterojunctions. However, the transition from the intrinsic semiconductor $BaZn_2As_2$ (BZA) to its doped compounds has not been extensively explored, especially in relation to the significant intermediate compound $Ba(Zn,Mn)_2As_2$ (BZMA). This study aims to address this gap by performing susceptibility and magnetization measurements, in addition to electronic transport analyses, on these compounds in their single crystal form. Key findings include the following: (1) carriers can significantly modulate the magnetism, transitioning from a non-magnetic BZA to a weak magnetic BZMA, and subsequently to a hard ferromagnet $(Ba,K)(Zn,Mn)_2As_2$ with potassium (K) doping to BZMA; (2) two distinct sets of metal-insulator transitions were identified, which can be elucidated by the involvement of carriers and the emergence of various magnetic states, respectively; and (3) BZMA exhibits colossal negative magnetoresistance, and by lanthanum (La) doping, a potential n-type $(Ba,La)(Zn,Mn)_2As_2$ single crystal was synthesized, demonstrating promising prospects for p-n junction applications. This study enhances our understanding of the magnetic interactions and evolutions among these compounds, particularly in the low-doping regime, thereby providing a comprehensive physical framework that complements previous findings related to the high-doping region.

Keywords: $BaZn_2As_2$; diluted magnetic semiconductors; metal–insulator transition; colossal negative magnetoresistance; anomalous hall effect

1. Introduction

The exploration and investigation of novel materials are critical components in the examination of the interaction between spin and charge in diluted magnetic semiconductors (DMSs) [1–4]. These materials demonstrate exceptional magnetic and electronic transport

properties [5–7] and hold significant potential for applications in spintronic devices [8–10]. Among the diverse range of materials, (Ga,Mn)As and its related systems [4,6,7,9–11] have functioned as a platform for investigating innovative concepts and the properties of DMSs in recent decades. However, this hetero-valent (Ga^{3+}/Mn^{2+}) doping severely limits solubility and necessitates the use of low-temperature molecular beam epitaxy techniques to obtain metastable films, which limits further development and study [4,6,9,10].

Since 2011, a new class of DMSs featuring independent spin and charge doping mechanisms [12,13] has sparked extensive research interest in the exploration of novel materials [14]. Among these new material systems, $BaZn_2As_2$ (BZA)-based DFSs [15–24] have garnered significant attention. It is important to note that the abbreviations for BZA and the related compounds presented herein are specifically applicable to this study. In comparison to the (Ga,Mn)As system, the $(BaK)(Zn,Mn)_2As_2$ (BKZMA) system offers several advantages: (i) it demonstrates a higher T_C, ranging from 180 K to 260 K [15,25,26], exceeding the T_C of (Ga,Mn)As, which is recorded at 200 K [7]; (ii) it provides the potential for multilayer heterojunctions in spintronic devices [15]; (iii) it allows for the synthesis of bulk and air-stable polycrystals and single crystals [1], thereby facilitating the application of various experimental techniques, including angle-resolved photoemission spectroscopy (ARPES) [16], neutron scattering measurements [21], and X-ray magnetic circular dichroism (XMCD) [19,23,24]; and (iv) it enables the independent manipulation of spins and charge doping, which may facilitate the differentiation of the distinct roles and effects of carriers and spins, thus allowing for an investigation of various magnetic states, including asperomagnetism [27]. Consequently, the BKZ system is established as a significant platform for future research endeavors [2,28]. However, the transition from the intrinsic semiconductor BZA to doped DMSs has not been extensively explored, especially in relation to the magnetic and electronic transport properties of significant intermediate compound $Ba(Zn,Mn)_2As_2$ (BZMA). In this study, we utilized a combination of magnetization measurements and electronic transport analyses on single crystals of BZA and doped compounds. Following the introduction, Section 2 will detail the materials and methods employed in this study. Section 3 will discuss the effects of doping on magnetic and electronic transport properties, as presented in the results and discussion section. Finally, the conclusions and outlook section will summarize the primary findings and propose possible directions for future research.

2. Materials and Methods

Single-crystal BZA and doped DMSs were fabricated via the flux method, which was shown in the previous report in detail [1,22]. Crystal structures were analyzed using X-ray powder diffraction with a Philips X'pert diffractometer and CuKα-radiation at the Institute of Physics, Chinese Academy of Siences (IoPCAS) in Beijing, China. The real compositions were determined by using energy-dispersive X-ray analysis (EDX) and inductively coupled plasma (ICP) mass spectrometry at the IoPCAS in Beijing China. Direct-current (dc) magnetic susceptibility was measured with a superconducting quantum interference device (SQUID) magnetometer(MPMS3, Quantum Design) at the IoPCAS in Beijing China, while electrical transport measurements were conducted on a physical property measurement system (PPMS, Quantum Design) and a JANIS He-4 refrigerator using a standard four-terminal method at the IoPCAS in Beijing China.

3. Results and Discussion

3.1. Crystal Structure Characterization

Figure 1a illustrates the crystal structure of the parent compound β-BZA, as well as the doped compounds, which are characterized by the space group I4/mmm [1,15]. These

compounds display alternating layers of barium (Ba), potassium (K), or lanthanum (La) and (Zn,Mn)As, which are formed from edge-sharing $ZnAs_4$ tetrahedra. This arrangement leads to a quasi-two-dimensional (2D) architecture. Consequently, the crystals could be readily cleaved into a plate-like shape, which represents the *ab*-plane. Furthermore, only the (0 0 2) series peaks were observed in the X-ray diffraction (XRD) patterns [1], as illustrated in Figure 1b.
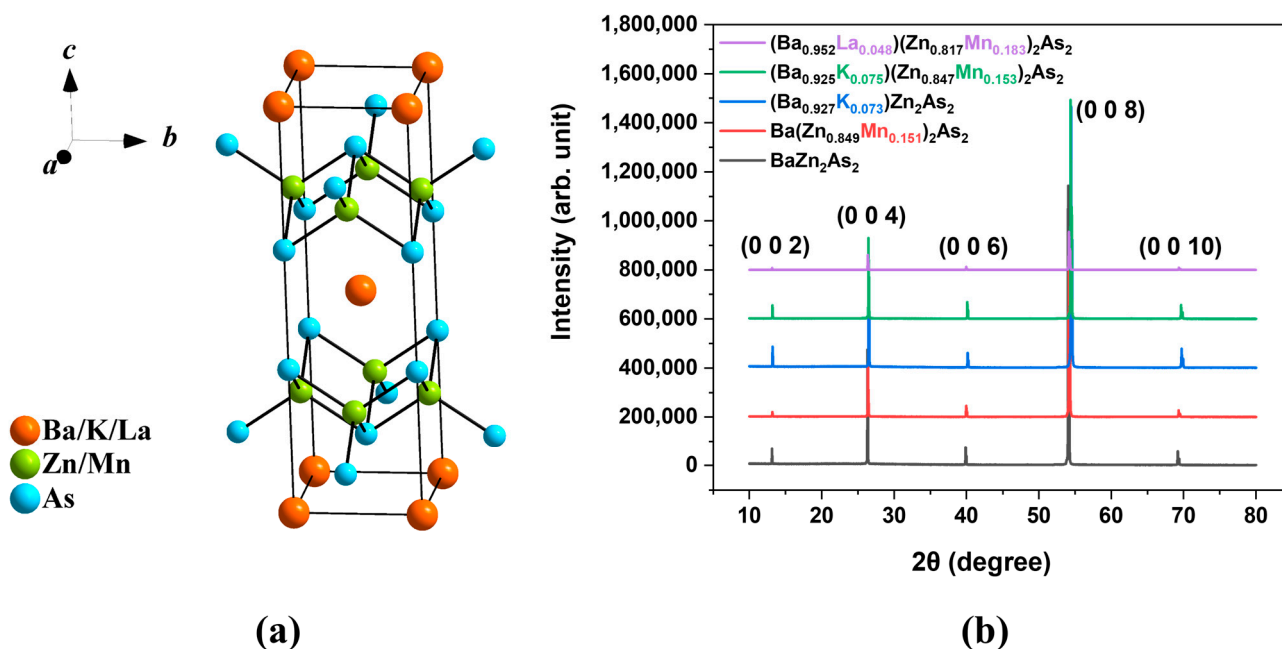

Figure 1. (**a**) The crystal structure of β-$BaZn_2As_2$ (BZA) and the doped compounds. (**b**) X-ray diffraction (XRD) pattern of the single-crystal samples.

3.2. Magnetic Susceptibility and Magnetization

Ideally, both the parent compound β-BZA and $(Ba_{0.927}K_{0.073})Zn_2As_2$ (BKZA) are non-magnetic. However, a trace amount of magnetic atoms may be introduced into these compounds, either from the raw elemental materials or during the fabrication process (for example, from the ceramic crucible used at 1200 °C [1]). Consequently, weak paramagnetic properties can be observed, as illustrated in Figure 2a,b. It is noteworthy that the curves for BZA and BKZA coincide. In Figure 2b, the magnetic intensity, measured with the unit of emu/g, was used to compare to the ferromagnetic (FM) DMSs $(Ba_{0.925}K_{0.075})(Zn_{0.847}Mn_{0.153})As_2$ (BKZMA), since both BZA and BKZA do not contain magnetic atoms. Similar properties were observed in the magnetization of BZA and the doped compounds when subjected to an external magnetic field perpendicular to the *c*-axis, as illustrated in Figure 3.

Figure 4a illustrates the dependence of carrier doping on the magnetic hysteresis curve $M(H)$, measured with the unit of μ_B/Mn, for doped compounds subjected to an external magnetic field along the *c*-axis at $T = 2$ K. As the K-doping level increases from zero in BZMA to 9.6% in BKZMA DMSs, the magnetic properties transition from weak magnets to a hard magnet, disregarding the minor differences in the Mn doping levels. Figure 4b presents a zoomed-in view of these results, which confirms the previous report in polycrystalline samples (see Figure 2c in reference [15]). This phenomenon is characteristic of carrier-mediated DFSs [29,30], wherein the carriers can modulate ferromagnetism to suppress antiferromagnetism through interactions between manganese (Mn) atoms. A similar phenomenon was also observed in other DFSs systems, such as PbSnMnTe [31], (In,Mn)As [32], and (Ge,Mn)Te [33]. This tendency can also be observed in the trend of change in various materials systems [34–39] in the Curie–Weiss temperature and the spin-

freezing temperature (T_f), as shown in Figures 2a and 3a, where the zero-field cooling (ZFC) magnetization significantly deviates from the field cooling (FC) magnetization. It is noteworthy that this deviation is not due to magnetic anisotropy, but rather exhibits spin-glass (SG) features [27,40], as a variety of material systems with polycrystalline states demonstrate this characteristic [34,36,41–49].
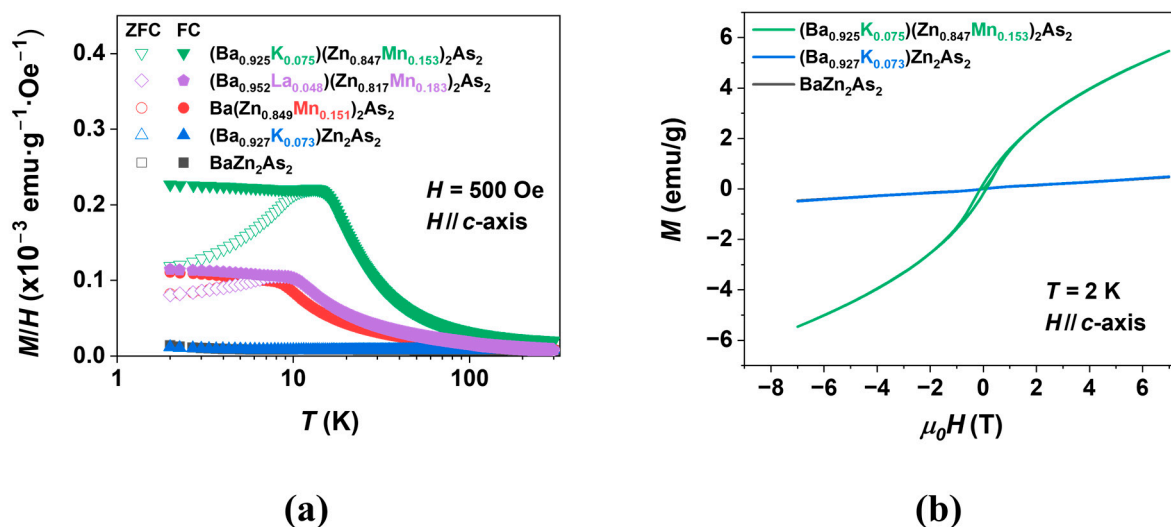

(a)   (b)

Figure 2. The effect of doping on the magnetic susceptibility measurements and magnetization of BaZn$_2$As$_2$ (BZA) and doped samples under an external magnetic field along the *c*-axis. (**a**) The direct-current (dc) magnetic susceptibility measurements were measured during zero-field cooling (ZFC, represented by open symbols) and field cooling (FC, represented by solid symbols) at a magnetic field of H = 500 Gauss (Oe); (**b**) the magnetic hysteresis curve $M(H)$ was obtained through field training and measured at a temperature of T = 2 K. It is noteworthy that the curves for BZA and (Ba$_{0.927}$K$_{0.073}$)Zn$_2$As$_2$ (BKZA) coincide in Figure 2a,b.
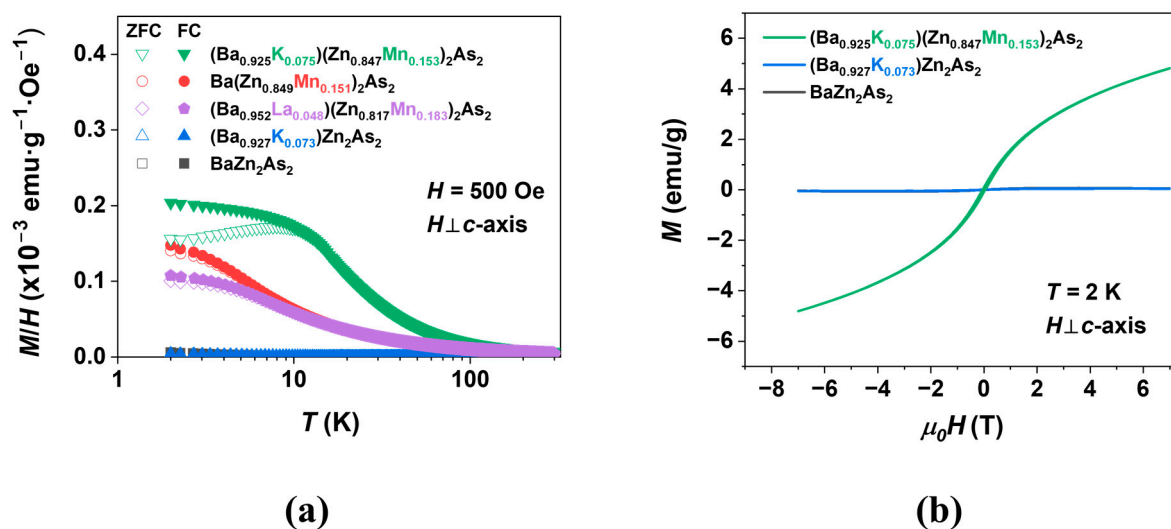

(a)   (b)

Figure 3. The effect of doping on the magnetic susceptibility measurements and magnetization of BaZn$_2$As$_2$ (BZA) and doped samples under an external magnetic field perpendicular to the *c*-axis. (**a**) The direct-current (dc) magnetic susceptibility measurements were taken during zero-field cooling (ZFC, represented by open symbols) and field cooling (FC, represented by solid symbols) at a magnetic field of H = 500 Gauss (Oe); (**b**) the magnetic hysteresis curve $M(H)$ was obtained through field training and measured at a temperature of T = 2 K. It is noteworthy that the curves for BZA and (Ba$_{0.927}$K$_{0.073}$)Zn$_2$As$_2$ (BKZA) coincide in Figure 3a,b.
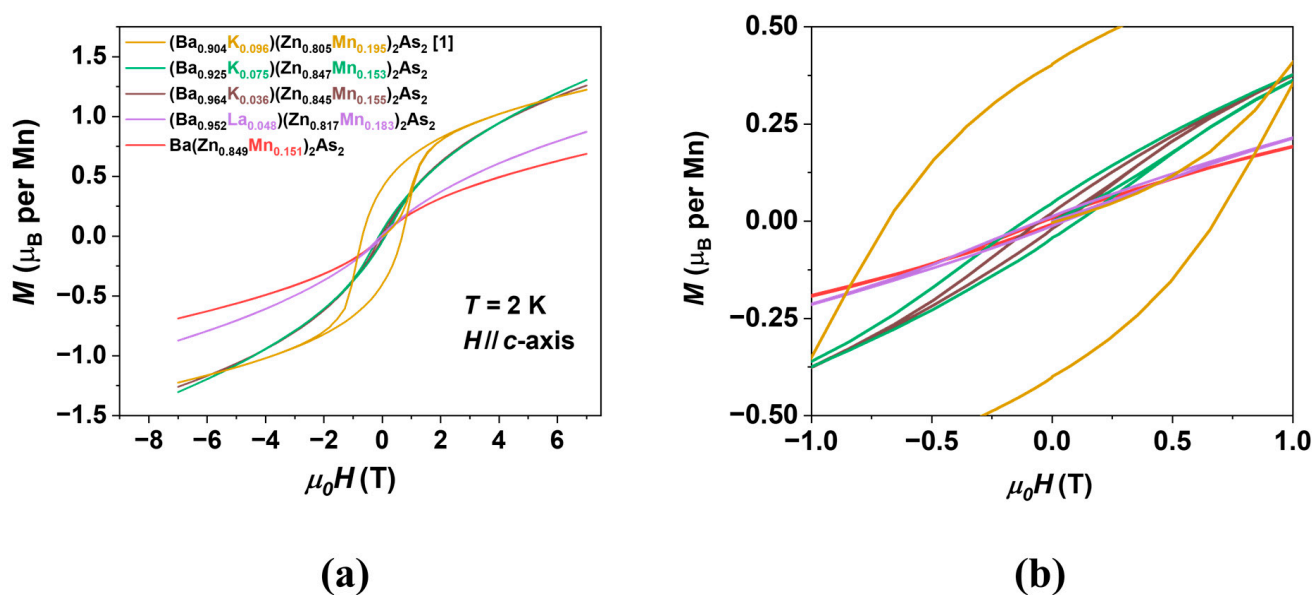
Figure 4. (**a**) The effect of carrier doping on the magnetic hysteresis curve *M*(*H*) of doped samples under the external magnetic field along the *c*-axis; (**b**) zoomed-in results.

However, the soft magnetic characteristics of small coercive forces were observed in the dependence of carrier doping on the magnetic hysteresis curve *M*(*H*) for doped samples subjected to an external magnetic field perpendicular to the *c*-axis at *T* = 2 K (Figure 5a). Notably, the coercive force gradually increases (Figure 5b). To clearly illustrate this phenomenon, we selectively chose two representative ferromagnetic (FM) samples to demonstrate the evolution of magnetic anisotropy, as shown in Figure 6. Two key findings are as follows: (1) the spin tends to align along the *c*-axis rather than the *ab*-plane; (2) the stronger the magnetism, the greater the magnetic anisotropy. This magnetic anisotropy could be explained by its magnetic structures and interactions [50–53].
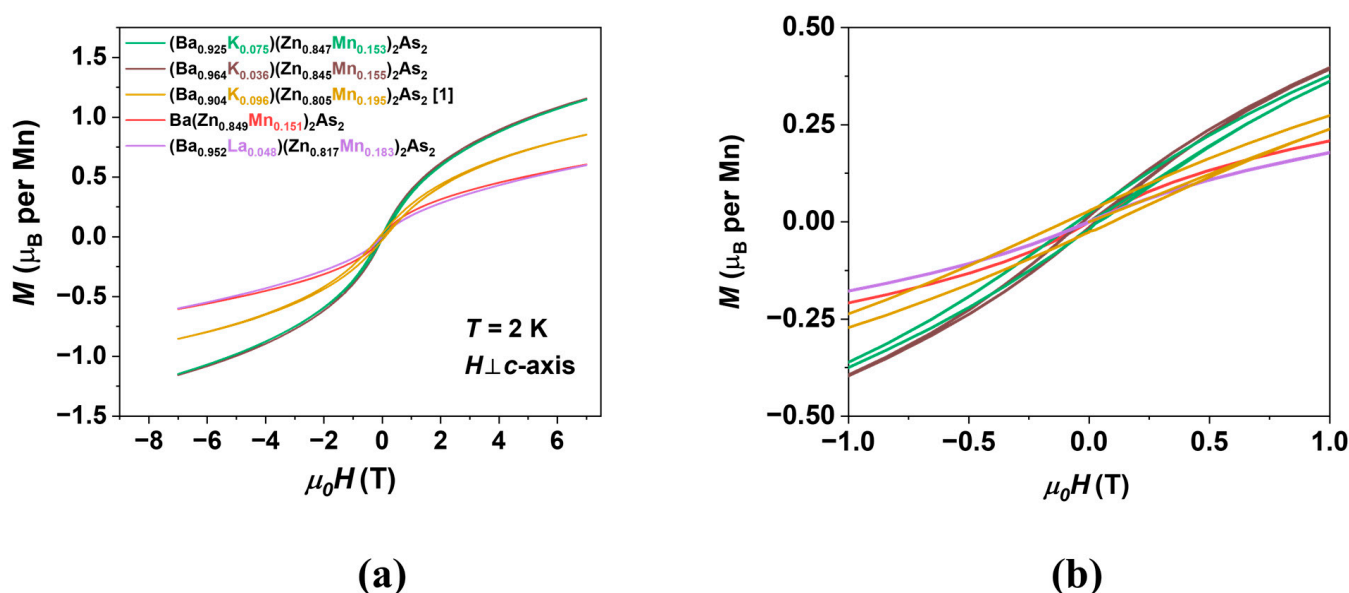

Figure 5. (**a**) The effect of carrier doping on the magnetic hysteresis curve *M*(*H*) of doped samples under the external magnetic field perpendicular to the *c*-axis; (**b**) zoomed-in results.
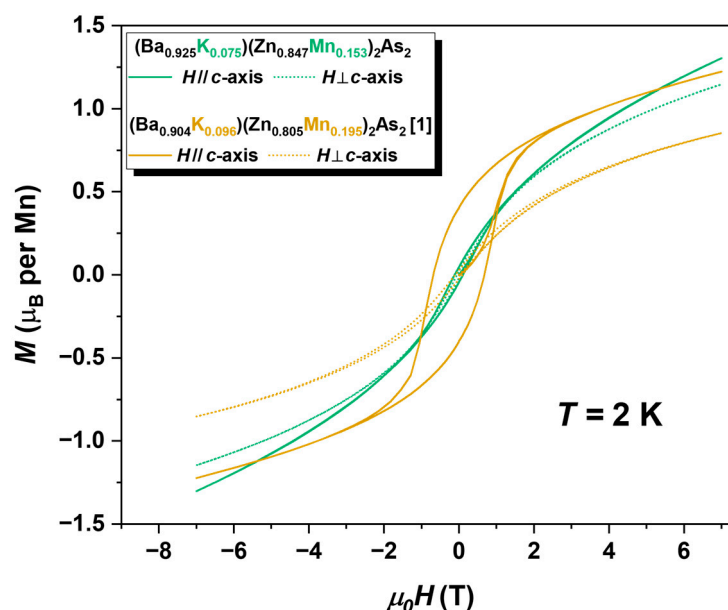
Figure 6. The magnetic hysteresis curve $M(H)$ measured at $T = 2$ K in different axes to exhibit magnetic anisotropy on both $(Ba_{0.925}K_{0.075})(Zn_{0.847}Mn_{0.153})_2As_2$ and $(Ba_{0.904}K_{0.096})(Zn_{0.805}Mn_{0.195})_2As_2$.

3.3. Electronic Transport Analyses

Comprehensive resistance analysis, magnetoresistance measurements, and Hall effect measurements were conducted to thoroughly investigate the interaction between magnetic and electronic transport properties in BZA systems. Figure 7a presents a schematic diagram of a typical four-point method used for electronic transport measurements. BZA and doped compounds were mechanically exfoliated into thin flakes with thicknesses ranging from 40 to 250 μm. To establish reliable Ohmic contacts, we utilized photoresist as a masking agent to define a Hall bar geometry on the pristine *ab*-plane of the samples. Subsequently, Cr/Au films (5 nm/100 nm) were deposited through electron-beam evaporation in an ultra-high-vacuum environment. Transport measurements were conducted utilizing a standard phase-sensitive four-terminal technique. A 100 μA AC excitation current with frequency f = 17.17 Hz current was applied in the *ab*-plane, while an external magnetic field was swept along the *c*-axis (perpendicular to the *ab*-plane). Both the longitudinal voltage (V_{xx}) and the Hall voltage (V_{xy}) were recorded simultaneously through two frequency-locked lock-in amplifiers to determine the corresponding longitudinal and Hall resistance of the sample. The magnetoresistance (ρ_{xx}) and the Hall resistance (ρ_{xy}) can be derived through symmetrized ($\rho_{xx}(B) = [\rho(B) + \rho(-B)]/2$) and antisymmetrized ($(\rho_{xy}(B) = [\rho(B) - \rho(-B)]/2)$) processing, respectively.

Figure 7b displays the temperature dependence of resistivity, measured from 2 K to 300 K, for four distinct samples under a zero magnetic field ($\mu_0 H = 0$ T). We observed a metal–insulator transition (MIT) from the intrinsic semiconductor BZA (black line) to the metallic BKZA (blue line) due to the introduction of hole carriers resulting from the substitution of Ba^{2+} with K^{1+}. The resistivity decreased by approximately two orders of magnitude. Notably, this phenomenon was also observed in various doped samples in a polycrystalline state, although the absolute resistivity of BZA is more than five orders of magnitude larger [15]. This disparity stems from the intrinsic properties of the polycrystalline sample and the electrode fabrication method. Grain boundaries in polycrystalline materials can hinder electron transport and increase resistivity. Additionally, the electrode fabrication process affects contact resistance; suboptimal contact may lead to overestimated resistivity values.
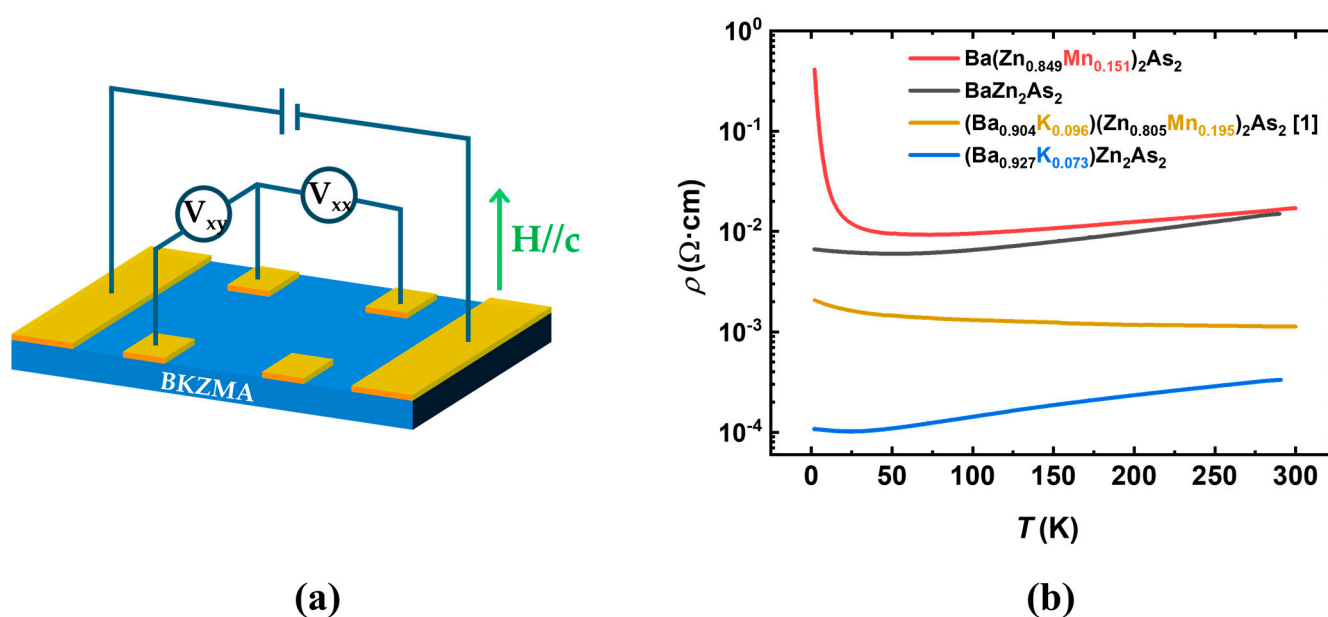
Figure 7. (**a**) The device schematic diagram of BZA and its doped compounds. The samples were fabricated to a Hall bar-like structure, which can measure the longitudinal and Hall components simultaneously. The external magnetic field was applied in a direction perpendicular to the *ab*-plane (or parallel to the *c*-axis). (**b**) The temperature dependence of the resistivities of four samples.

Most significantly, the involvement of spin through Zn^{2+}/Mn^{2+} ions induces another metal–insulator transition, transitioning from the metallic BKZA (blue line) to the semiconducting BKZMA (brown line), suggesting the opening of an energy gap in the electronic band structure. This transition is primarily attributed to the presence of the magnetic element Mn^{2+}, and its effects. This phenomenon can be further elucidated by comparing the transition from BZA to BZMA (red line), consistent with Anderson localization mediated by the disordered potential of Mn dopants.

Figure 8 presents the magnetoresistance (MR) and Hall effect measurements for BZMA. The raw data have been symmetrized and antisymmetrized to extract the independent two components, where MR is defined as MR = $[\rho(\mu_0 H) - \rho(0)]/\rho(0) \times 100\%$. As shown in Figure 8a, BZMA exhibits negative magnetoresistance, reaching -96.3% at 2 K and 5 T. This phenomenon originates from magnetic impurity scattering. The negative MR weakens progressively with increasing temperature, diminishing to only -1.47% at 75 K and 5 T. Ideally, BZA and BZMA have a close carrier concentration since Zn^{2+}/Mn^{2+} is an equivalent substitution. Consequently, BZMA shows a paramagnetic property, as predicted by the carrier-mediated DMSs systems [29,30]. However, it exhibits weak magnetic properties, specifically as a spin glass or weak ferromagnet, with a freezing temperature of approximately 10 K, as illustrated in Figures 2a and 3a. This behavior is attributed to the additional charge carriers introduced by defects, such as interstitial manganese (Mn) ions. The anomalous Hall effect (AHE) further supports these observations, as depicted in Figure 8b. The Hall curve demonstrates nonlinear behavior due to the superposition of the ordinary Hall effect (which is linear in the magnetic field) and the AHE (which is proportional to magnetization). As the temperature increases, the reduced magnetization diminishes the contribution of the AHE, resulting in a predominantly linear field dependence that is dominated by the ordinary Hall effect.
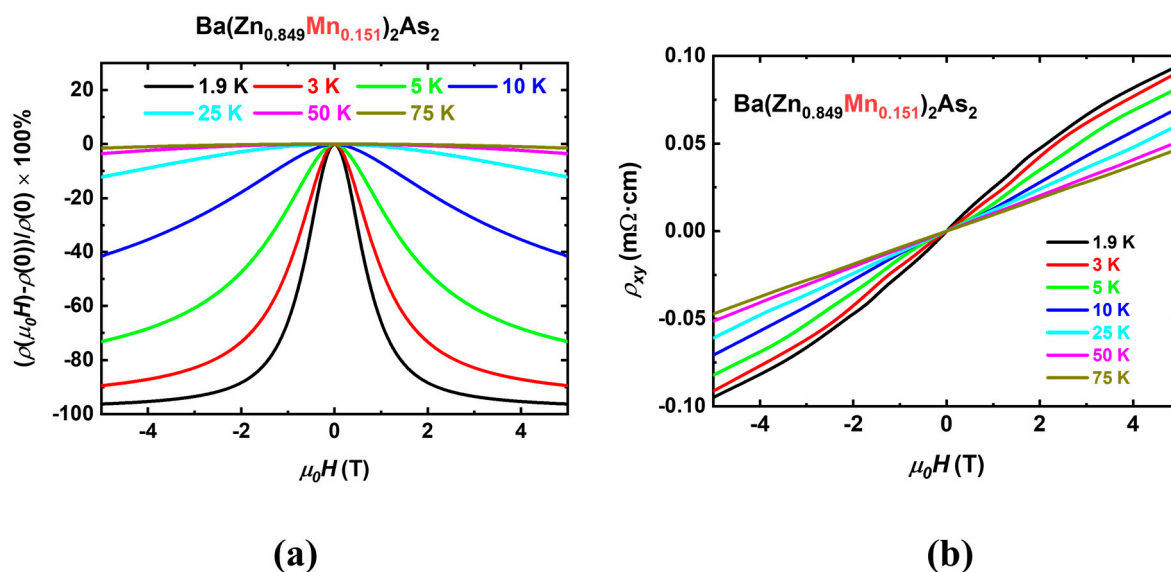
(a)

(b)

Figure 8. The magnetoresistance (**a**) and Hall resistivity (**b**) curves of Ba(Zn$_{0.849}$Mn$_{0.151}$)$_2$As$_2$ at varied temperatures.

Figure 9 shows a comparative study of the magneto-transport properties among four distinct compounds. The parent compound BZA exhibits a weak negative MR of approximately -1.24% at 10 K and 5 T, indicative of limited spin-dependent scattering channels. Remarkably, Mn doping in BZMA dramatically enhances the negative MR to -41.47% under identical conditions, demonstrating the crucial role of spin polarization introduced by Mn^{2+} ions. Intriguingly, additional K doping in BKZMA leads to a moderated MR effect, suggesting competing mechanisms between carrier doping-induced metallicity and long-range ferromagnetic ordering. The solely K-doped BKZA displays a nearly negligible MR, consistent with its enhanced metallic character. This doping-dependent evolution is further corroborated by Hall measurements, where only the Mn-containing compounds exhibit AHE, a hallmark of ferromagnetic ordering. Notably, the consistently positive Hall coefficients across all compositions unambiguously confirm hole-dominated conduction in this material system.
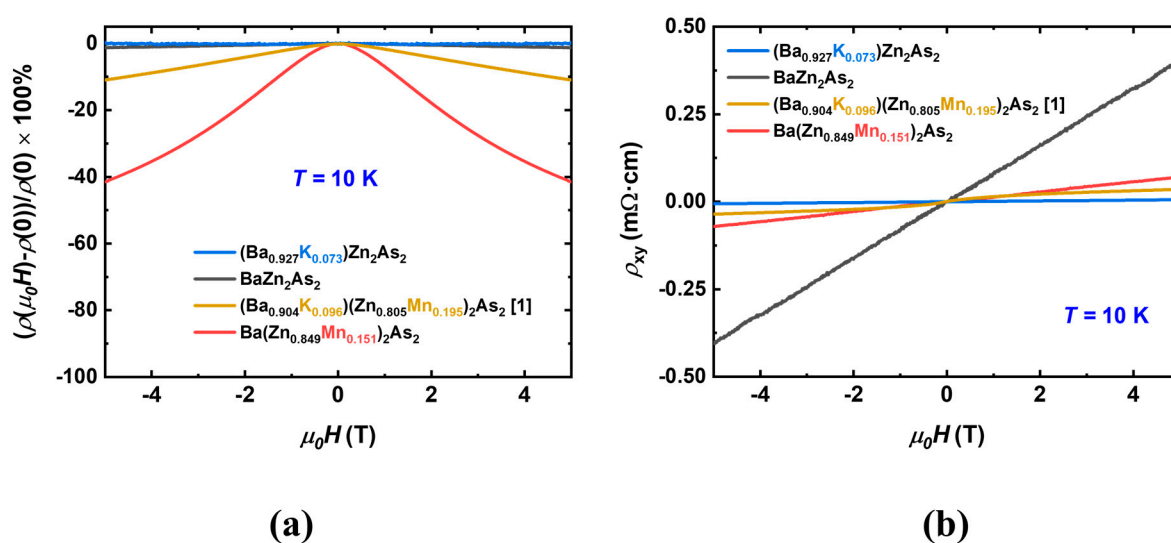

(a)

(b)

Figure 9. The magnetoresistance (**a**) and Hall resistivities (**b**) of BZA, BKZA, BZMA, and BKZMA at T = 10 K.

The hole carrier densities (n_p) of four compounds, obtained through the linear fitting of Hall curves under high magnetic fields as a function of temperature, are illustrated in Figure 10. For the parent compound BZA, n_p shows a gradual increase as the temperature decreases, reflecting its intrinsic semiconducting behavior. In contrast, both BZMA and BKZMA exhibit an opposite trend, with a significant reduction in n_p at lower temperatures. The solely K-doped BKZA demonstrates nearly temperature-independent carrier densities, consistent with its highly metallic character. Notably, K doping enhances n_p by nearly two orders of magnitude compared to the undoped compound, as evidenced by the substantial difference between BKZA (n_p~10^{20} cm^{-3}) and BZA (n_p~10^{19} cm^{-3}). This carrier enhancement effect is also observed in Mn-containing systems; at comparable manganese doping levels, BKZMA displays a significantly higher n_p than BZMA. This observation underscores the predominant role of carriers in modulating ferromagnetism, which in turn suppresses antiferromagnetism through the interactions between Mn atoms, in agreement with theoretical explanations in the BZA system [50–52].
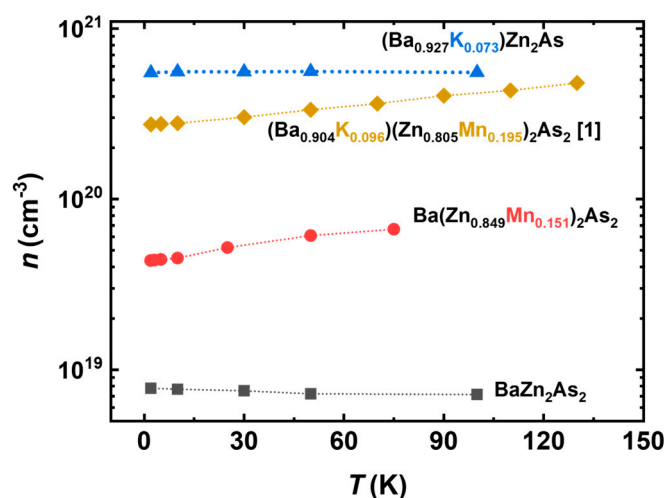

Figure 10. Temperature dependence of carrier densities of BZA, BKZA, BZMA, and BKZMA at $T = 10$ K.

The fabrication of a p-n junction within a single materials system represents a long-term objective in the field of materials science. This study investigates the potential of (Ba,La)(Zn,Mn)$_2$As$_2$ (BLZMA) for this purpose. Typically, the stable oxidation state of La is +3, which allows us to introduce electron carriers through the Ba^{2+}/La^{3+} substitution mechanism. As anticipated in previous studies [29,30], the magnetic interactions mediated by electron carriers are significantly weaker than those associated with hole carriers, primarily due to the lower effective mass of the electrons. Consequently, it is expected that *n*-type dilute magnetic semiconductors (DMSs) will exhibit weaker magnetic properties compared to their *p*-type counterparts, assuming equivalent carrier concentrations. As illustrated in Figures 2–5, the magnetism of BLZMA is weaker than that of BKZMA. Although the Hall effect could be employed to confirm the n-type properties of BLZMA, the small size of the BLZMA samples currently limits the fabrication of Hall electrodes. Future efforts will focus on improving fabrication techniques to grow larger single-crystal BLZMA or adapting micro-nano technology to conduct this experiment.

4. Conclusions and Outlook

We conducted a comprehensive study on BZA and its doped compounds, employing a variety of techniques. The investigation into the magnetic evolution and electronic transport properties provided detailed insights into the magnetic interactions within BZA systems.

Future research is expected to include Hall measurements and the examination of various junctions in BZA systems [2] with the aim of exploring the potential for spin-dependent phenomena and innovative device concepts [8–10].

Conflicts of Interest: The authors declare no conflicts of interest.

References

1. Zhao, G.Q.; Lin, C.J.; Deng, Z.; Gu, G.X.; Yu, S.; Wang, X.C.; Gong, Z.Z.; Uemura, Y.J.; Li, Y.Q.; Jin, C.Q. Single crystal growth and spin polarization measurements of diluted magnetic semiconductor (BaK)(ZnMn)$_2$As$_2$. *Sci. Rep.* **2017**, *7*, 14473. [CrossRef]
2. Žutić, I.; Zhou, T. Tailoring magnetism in semiconductors. *Sci. China Phys. Mech. Astron.* **2018**, *61*, 067031. [CrossRef]
3. Furdyna, J.K. Diluted magnetic semiconductors. *J. Appl. Phys.* **1988**, *64*, R29–R64. [CrossRef]
4. Dietl, T.; Bonanni, A.; Ohno, H. Families of magnetic semiconductors—An overview. *J. Semicond.* **2019**, *40*, 080301. [CrossRef]
5. Coey, J.M.D. *Magnetism and Magnetic Materials*; Cambridge University Press: Cambridge, UK, 2010.
6. Jungwirth, T.; Sinova, J.; Mašek, J.; Kučera, J.; MacDonald, A.H. Theory of ferromagnetic (III,Mn)V semiconductors. *Rev. Mod. Phys.* **2006**, *78*, 809–864. [CrossRef]
7. Chen, L.; Yang, X.; Yang, F.; Zhao, J.; Misuraca, J.; Xiong, P.; von Molnar, S. Enhancing the curie temperature of ferromagnetic semiconductor (Ga,Mn)As to 200 K via nanostructure engineering. *Nano Lett.* **2011**, *11*, 2584–2589. [CrossRef] [PubMed]
8. Žutić, I.; Fabian, J.; Sarma, S.D. Spintronics fundamentals and applications. *Rev. Mod. Phys.* **2004**, *76*, 323. [CrossRef]
9. Jungwirth, T.; Wunderlich, J.; Novák, V.; Olejník, K.; Olejník, K.; Gallagher, B.L.; Campion, R.P.; Edmonds, K.W. Spin-dependent phenomena and device concepts explored in (Ga,Mn)As. *Rev. Mod. Phys.* **2014**, *86*, 855–896. [CrossRef]
10. Dietl, T.; Ohno, H. Dilute ferromagnetic semiconductors: Physics and spintronic structures. *Rev. Mod. Phys.* **2014**, *86*, 187–251. [CrossRef]
11. Ohno, H.; Shen, A.; Matsukura, F.; Oiwa, A.; Endo, A.; Katsumoto, S.; Iye, Y. (Ga,Mn)As: A new diluted magnetic semiconductor based on GaAs. *Appl. Phys. Lett.* **1996**, *69*, 363–365. [CrossRef]
12. Deng, Z.; Jin, C.Q.; Liu, Q.Q.; Wang, X.C.; Zhu, J.L.; Feng, S.M.; Chen, L.C.; Yu, R.C.; Arguello, C.; Goko, T.; et al. Li(Zn,Mn)As as a new generation ferromagnet based on a I-II-V semiconductor. *Nat. Commun.* **2011**, *2*, 422. [CrossRef] [PubMed]
13. Masek, J.; Kudrnovsky, J.; Maca, F.; Gallagher, B.L.; Campion, R.P.; Gregory, D.H.; Jungwirth, T. Dilute moment *n*-type ferromagnetic semiconductor Li(Zn,Mn)As. *Phys. Rev. Lett.* **2007**, *98*, 067202. [CrossRef]
14. Zhao, G.; Deng, Z.; Jin, C. Advances in new generation diluted magnetic semiconductors with independent spin and charge doping. *J. Semicond.* **2019**, *80*, 081505. [CrossRef]

15. Zhao, K.; Deng, Z.; Wang, X.C.; Han, W.; Zhu, J.L.; Li, X.; Liu, Q.Q.; Yu, R.C.; Goko, T.; Frandsen, B.; et al. New diluted ferromagnetic semiconductor with curie temperature up to 180 K and isostructural to the '122' iron-based superconductors. *Nat. Commun.* **2013**, *4*, 1442. [CrossRef]

16. Suzuki, H.; Zhao, G.Q.; Zhao, K.; Chen, B.J.; Horio, M.; Koshiishi, K.; Xu, J.; Kobayashi, M.; Minohara, M.; Sakai, E.; et al. Fermi surfaces and $p-d$ hybridization in the diluted magnetic semiconductor $Ba_{1-x}K_x(Zn_{1-y}Mn_y)_2As_2$ studied by soft x-ray angle-resolved photoemission spectroscopy. *Phys. Rev. B* **2015**, *92*, 235120. [CrossRef]

17. Sun, F.; Xu, C.; Yu, S.; Chen, B.-J.; Zhao, G.-Q.; Deng, Z.; Yang, W.-G.; Jin, C.-Q. Synchrotron x-ray diffraction studies on the new generation ferromagnetic semiconductor Li(Zn,Mn)As under high pressure. *Chin. Phys. Lett.* **2017**, *34*, 067501. [CrossRef]

18. Suzuki, H.; Zhao, K.; Shibata, G.; Takahashi, Y.; Sakamoto, S.; Yoshimatsu, K.; Chen, B.J.; Kumigashira, H.; Chang, F.H.; Lin, H.J.; et al. Photoemission and x-ray absorption studies of the isostructural to Fe-based superconductors diluted magnetic semiconductor $(Ba_{1-x}K_x)(Zn_{1-y}Mn_y)_2As_2$. *Phys. Rev. B* **2015**, *91*, 140401. [CrossRef]

19. Sun, F.; Zhao, G.Q.; Escanhoela, C.A.; Chen, B.J.; Kou, R.H.; Wang, Y.G.; Xiao, Y.M.; Chow, P.; Mao, H.K.; Haskel, D.; et al. Hole doping and pressure effects on the II-II-V-based diluted magnetic semiconductor $(Ba_{1-x}K_x)(Zn_{1-y}Mn_y)_2As_2$. *Phys. Rev. B* **2017**, *95*, 094412. [CrossRef]

20. Wang, R.; Huang, Z.X.; Zhao, G.Q.; Yu, S.; Deng, Z.; Jin, C.Q.; Jia, Q.J.; Chen, Y.; Yang, T.Y.; Jiang, X.M.; et al. Out-of-plane easy-axis in thin films of diluted magnetic semiconductor $Ba_{1-x}K_x(Zn_{1-y}Mn_y)_2As_2$. *AIP Adv.* **2017**, *7*, 045017. [CrossRef]

21. Surmach, M.A.; Chen, B.J.; Deng, Z.; Jin, C.Q.; Glasbrenner, J.K.; Mazin, I.I.; Ivanov, A.; Inosov, D.S. Weak doping dependence of the antiferromagnetic coupling between nearest-neighbor Mn^{2+} spins in $(Ba_{1-x}K_x)(Zn_{1-y}Mn_y)_2As_2$. *Phys. Rev. B* **2018**, *97*, 104418. [CrossRef]

22. Zhao, G.Q.; Li, Z.; Sun, F.; Yuan, Z.; Chen, B.J.; Yu, S.; Peng, Y.; Deng, Z.; Wang, X.C.; Jin, C.Q. Effects of high pressure on the ferromagnetism and in-plane electrical transport of $(Ba_{0.904}K_{0.096})(Zn_{0.805}Mn_{0.195})_2As_2$ single crystal. *J. Phys. Condens. Matter* **2018**, *30*, 254001. [CrossRef] [PubMed]

23. Suzuki, H.; Zhao, G.; Okamoto, J.; Sakamoto, S.; Chen, Z.-Y.; Nonaka, Y.; Shibata, G.; Zhao, K.; Chen, B.; Wu, W.-B.; et al. Magnetic properties and electronic configurations of Mn ions in the diluted magnetic semiconductor $Ba_{1-x}K_x(Zn_{1-y}Mn_y)_2As_2$ studied by x-ray magnetic circular dichroism and resonant inelastic x-ray scattering. *J. Phys. Soc. Jpn.* **2022**, *91*, 064710. [CrossRef]

24. Sakamoto, S.; Zhao, G.Q.; Shibata, G.; Deng, Z.; Zhao, K.; Wang, X.C.; Nonaka, Y.; Ikeda, K.; Chi, Z.D.; Wan, Y.X.; et al. Anisotropic spin distribution and perpendicular magnetic anisotropy in a layered ferromagnetic semiconductor $(Ba,K)(Zn,Mn)_2As_2$. *ACS Appl. Electron. Mater.* **2021**, *3*, 789–794. [CrossRef]

25. Zhao, K.; Chen, B.; Zhao, G.; Yuan, Z.; Liu, Q.; Deng, Z.; Zhu, J.; Jin, C. Ferromagnetism at 230 K in $(Ba_{0.7}K_{0.3})(Zn_{0.85}Mn_{0.15})_2As_2$ diluted magnetic semiconductor. *Chin. Sci. Bull.* **2014**, *59*, 2524–2527. [CrossRef]

26. Peng, Y.; Li, X.; Shi, L.; Zhao, G.; Zhang, J.; Zhao, J.; Wang, X.; Gu, B.; Deng, Z.; Uemura, Y.J.; et al. A near room temperature curie temperature in a new type of diluted magnetic semiconductor $(Ba,K)(Zn,Mn)_2As_2$. *Adv. Phys. Res.* **2024**, *4*, 2400124. [CrossRef]

27. Zhao, G.; Cai, Y.; Kojima, K.M.; Sheng, Q.; Beare, J.; Luke, G.; Li, X.; Peng, Y.; Ziman, T.; Zhao, K.; et al. Magnetic evolution of carrier doping and spin dynamics in diluted magnetic semiconductors $(Ba,Na)(Zn,Mn)_2As_2$. *Condens. Matter* **2025**, *10*, 30. [CrossRef]

28. Hirohata, A.; Sukegawa, H.; Yanagihara, H.; Zutic, I.; Seki, T.; Mizukami, S.; Swaminathan, R. Roadmap for emerging materials for spintronic device applications. *IEEE Trans. Magn.* **2015**, *51*, 0800511. [CrossRef]

29. Dietl, T.; Ohno, H.; Matsukura, F.; Cibert, J.; Ferrand, D. Zener model description of ferromagnetism in zinc-blende magnetic semiconductors. *Science* **2000**, *287*, 1019–1022. [CrossRef]

30. Dietl, T.; Ohno, H.; Matsukura, F. Hole-mediated ferromagnetism in tetrahedrally coordinated semiconductors. *Phys. Rev. B* **2001**, *63*, 195205. [CrossRef]

31. Story, T.; Galazka, R.R.; Frankel, R.B.; Wolff, P.A. Carrier-concentration-induced ferromagnetism in pbsnmnte. *Phys. Rev. Lett.* **1986**, *56*, 777–779. [CrossRef]

32. Koshihara, S.; Oiwa, A.; Hirasawa, M.; Katsumoto, S.; Iye, Y.; Urano, C.; Takagi, H.; Munekata, H. Ferromagnetic order induced by photogenerated carriers in magnetic III-V semiconductor heterostructures of (In,Mn)As/GaSb. *Phys. Rev. Lett.* **1997**, *78*, 4617–4620. [CrossRef]

33. Fukuma, Y.; Asada, H.; Miyawaki, S.; Koyanagi, T.; Senba, S.; Goto, K.; Sato, H. Carrier-induced ferromagnetism in $Ge_{0.92}Mn_{0.08}Te$ epilayers with a Curie temperature up to 190 K. *Appl. Phys. Lett.* **2008**, *93*, 252502. [CrossRef]

34. Ding, C.; Gong, X.; Man, H.; Zhi, G.; Guo, S.; Zhao, Y.; Wang, H.; Chen, B.; Ning, F.L. The suppression of curie temperature by Sr doping in diluted ferromagnetic semiconductor $(La_{1-x}Sr_x)(Zn_{1-y}Mn_y)AsO$. *EPL (Europhys. Lett.)* **2014**, *107*, 17004. [CrossRef]

35. Man, H.; Guo, S.; Sui, Y.; Guo, Y.; Chen, B.; Wang, H.; Ding, C.; Ning, F.L. $Ba(Zn_{1-2x}Mn_xCu_x)_2As_2$: A bulk form diluted ferromagnetic semiconductor with Mn and Cu codoping at Zn sites. *Sci. Rep.* **2015**, *5*, 15507. [CrossRef]

36. Guo, S.; Man, H.; Gong, X.; Ding, C.; Zhao, Y.; Chen, B.; Guo, Y.; Wang, H.; Ning, F.L. $(Ba_{1-x}K_x)(Cu_{2-x}Mn_x)Se_2$: A copper-based bulk form diluted magnetic semiconductor with orthorhombic $BaCu_2S_2$-type structure. *J. Magn. Magn. Mater.* **2016**, *400*, 295–299. [CrossRef]

37. Gu, Y.; Zhang, H.; Zhang, R.; Fu, L.; Wang, K.; Zhi, G.; Guo, S.; Ning, F. A novel diluted magnetic semiconductor (Ca,Na)(Zn,Mn)$_2$Sb$_2$ with decoupled charge and spin dopings. *Chin. Phys. B* **2020**, *29*, 057507. [CrossRef]

38. Yu, S.; Zhao, G.; Peng, Y.; Wang, X.; Liu, Q.; Yu, R.; Zhang, S.; Zhao, J.; Li, W.; Deng, Z.; et al. (Ba,K)(Zn,Mn)$_2$Sb$_2$: A new type of diluted magnetic semiconductor. *Crystals* **2020**, *10*, 690. [CrossRef]

39. Gu, Y.; Zhang, R.; Zhang, H.; Fu, L.; Zhi, G.; Dong, J.; Zhao, X.; Xie, L.; Ning, F. A CaAl$_2$Si$_2$-type magnetic semiconductor (Sr,Na)(Zn,Mn)$_2$Sb$_2$ isostructural to 122-type iron-based superconductors. *Adv. Condens. Matter Phys.* **2022**, *2022*, 4291923. [CrossRef]

40. Gu, G.; Zhao, G.; Lin, C.; Li, Y.; Jin, C.; Xiang, G. Asperomagnetic order in diluted magnetic semiconductor (Ba,Na)(Zn,Mn)$_2$As$_2$. *Appl. Phys. Lett.* **2018**, *112*, 032402. [CrossRef]

41. Guo, S.L.; Zhao, Y.; Man, H.Y.; Ding, C.; Gong, X.; Zhi, G.X.; Fu, L.C.; Gu, Y.L.; Frandsen, B.A.; Liu, L.; et al. μSR investigation of a new diluted magnetic semiconductor Li(Zn,Mn,Cu)As with Mn and Cu codoping at the same Zn sites. *J. Phys. Condens. Matter* **2016**, *28*, 366001. [CrossRef]

42. Yu, S.; Peng, Y.; Zhao, G.; Zhao, J.; Wang, X.; Zhang, J.; Deng, Z.; Jin, C. Colossal negative magnetoresistance in spin glass Na(Zn,Mn)Sb. *J. Semicond.* **2023**, *44*, 032501. [CrossRef]

43. Lu, J.; Man, H.; Ding, C.; Wang, Q.; Yu, B.; Guo, S.; Wang, H.; Chen, B.; Han, W.; Jin, C.; et al. The synthesis and characterization of 1111-type diluted magnetic semiconductors (La$_{1−x}$Sr$_x$)(Zn$_{1−x}$TM$_x$)AsO (Tm = Mn, Fe, Co). *EPL (Europhys. Lett.)* **2013**, *103*, 67011. [CrossRef]

44. Zhao, X.D.; Dong, J.O.; Fu, L.C.; Gu, Y.L.; Zhang, R.F.; Yang, Q.L.; Xie, L.F.; Tang, Y.S.; Ning, F.L. (Ba$_{1−x}$Na$_x$)F(Zn$_{1−X}$Mn$_x$)Sb: A novel fluoride-antimonide magnetic semiconductor with decoupled charge and spin doping. *J. Semicond.* **2022**, *43*, 112501. [CrossRef]

45. Fu, L.; Gu, Y.; Guo, S.; Wang, K.; Zhang, H.; Zhi, G.; Liu, H.; Xu, Y.; Wang, Y.; Wang, H.; et al. Ferromagnetism in fluoride-antimonide SrF(Zn$_{1-2x}$Mn$_x$Cu$_x$)Sb with a quasi two dimensional structure. *J. Magn. Magn. Mater.* **2019**, *483*, 95–99. [CrossRef]

46. Ding, C.; Man, H.; Qin, C.; Lu, J.; Sun, Y.; Wang, Q.; Yu, B.; Feng, C.; Goko, T.; Arguello, C.J.; et al. (La$_{1−x}$Ba$_x$)(Zn$_{1−x}$Mn$_x$)AsO: A two-dimensional 1111-type diluted magnetic semiconductor in bulk form. *Phys. Rev. B* **2013**, *88*, 041102. [CrossRef]

47. Han, W.; Zhao, K.; Wang, X.; Liu, Q.; Ning, F.; Deng, Z.; Liu, Y.; Zhu, J.; Ding, C.; Man, H.; et al. Diluted ferromagnetic semiconductor (LaCa)(ZnMn)SbO isostructural to "1111" type iron pnictide superconductors. *Sci. China Phys. Mech. Astron.* **2013**, *56*, 2026–2030. [CrossRef]

48. Ding, C.; Guo, S.; Zhao, Y.; Man, H.; Fu, L.; Gu, Y.; Wang, Z.; Liu, L.; Frandsen, B.A.; Cheung, S.; et al. The synthesis and characterization of 1111 type diluted ferromagnetic semiconductor (La$_{1−x}$Ca$_x$)(Zn$_{1−x}$Mn$_x$)AsO. *J. Phys. Condens. Matter* **2016**, *28*, 026003. [CrossRef]

49. Zhang, R.; Xu, C.; Fu, L.; Gu, Y.; Zhi, G.; Dong, J.; Zhao, X.; Xie, L.; Zhang, H.; Cao, C.; et al. Manipulation of the ferromagnetic ordering in magnetic semiconductor (La,Ca)(Zn,Mn)AsO by chemical pressure. *J. Magn. Magn. Mater.* **2022**, *554*, 169276. [CrossRef]

50. Glasbrenner, J.K.; Mazin, I.I. First-principles evidence of Mn moment canting in hole-doped Ba$_{1−2x}$K$_{2x}$Mn$_2$As$_2$. *Phys. Rev. B* **2014**, *89*, 060403. [CrossRef]

51. Glasbrenner, J.K.; Žutić, I.; Mazin, I.I. Theory of Mn-doped II-II-V semiconductors. *Phys. Rev. B* **2014**, *90*, 140403. [CrossRef]

52. Gu, B.; Maekawa, S. Diluted magnetic semiconductors with narrow band gaps. *Phys. Rev. B* **2016**, *94*, 155202. [CrossRef]

53. Gu, B.; Maekawa, S. New p- and n-type ferromagnetic semiconductors: Cr-doped BaZn$_2$As$_2$. *AIP Adv.* **2017**, *7*, 055805. [CrossRef]